CRITICAL REVIEW

Electron beam powder bed fusion of copper components: a review of mechanical properties and research opportunities

Elmira Sharabian[1,2] · Martin Leary[2] · Darren Fraser[1] · Stefan Gulizia[1]

Abstract

The purpose of this work is to identify the principle of electron beam powder bed fusion (EB-PBF) and the performance of this AM method in the processing of copper components. This review details the experimentally reported properties, including microstructural, mechanical and physical properties of pure copper made by EB-PBF. The technical challenges and opportunities of EB-PBF are identified to provide insight into the influence of process parameters on observed mechanical properties as well as a roadmap for strategic research opportunities in this field. These insights allow optimisation of EB-PBF parameters, as well as comparison of the relative merits of EB-PBF over LB-PBF in the processing of copper components. This review details the microstructure and mechanical properties of EB-PBF of copper and identifies the technical opportunities and challenges. In addition, this report characterises the influence of process parameters, and subsequent energy density, on the associated mechanical properties. The discussions showed that the chance of pollution in copper processing by EB-PBF is less than laser-based powder bed fusion (LB-PBF) due to the high vacuum environment for electron beam. Oxygen content in the EB-PBF of copper powder is a vital factor and significantly affects the mechanical properties and quality of the specimen including physical density. The produced Cu_2O due to the existence of oxygen content (in powder and bulk material) can improve the mechanical properties. However, if the Cu_2O exceeds a certain percentage (0.0235%wt), cracks appear and negatively affect the mechanical properties. In copper printing by this method, the process parameters have to be tuned in such a way as to generate low build temperatures due to the high thermal conductivity of this alloy and the high sintering tendency of the powder.

Keywords Electron beam powder bed fusion · Copper · Mechanical properties · Process parameter

1 Introduction

Additive manufacturing (AM) refers to a category of manufacturing processes that sequentially add layers or units of standard input materials to enable the production of physical products. This process was previously called rapid prototyping but is now applied in three dimensions and leads to the commonly applied terminology, 3D printing.

By this simple definition, AM processes have existed for centuries, for instance, in the form of common brick (laying) used for the building of complex structures. A commercially relevant explanation of AM must also include a restriction that this technology is digitally driven, whereby AM is enabled by digital definitions of the planned geometry and related process parameters. This qualification enables the diverse range of sophisticated design outcomes related to modern AM processes, comprising high-complexity customised 3D structures, inexpensive functional components, high-value structures systems and inexpensive, fully customised patient-specific surgical guides [1, 2].

A common initial definition of 3D printing was to produce the objects in three dimensions using droplets, while some processes such as friction stir additive manufacturing,

✉ Elmira Sharabian
  s3913935@student.rmit.edu.au

  Martin Leary
  martin.leary@rmit.edu.au

  Darren Fraser
  darren.fraser@csiro.au

  Stefan Gulizia
  stefan.gulizia@csiro.au

1   CSIRO Manufacturing, Clayton, VIC 3168, Australia

2   Centre for Additive Manufacturing, School of Engineering, Royal Melbourne Institute of Technology, Melbourne, VIC, Australia

sheet lamination and cold spray produce 3D shapes without droplets. Therefore, a technical committee of ASTM International arrived at the decision to make a novel terminology to be adopted and cover all possible processes. As a result, ASTM [3] agreement standards now use the term additive manufacturing as do most standards bodies worldwide.

Powder bed fusion (PBF) is one of the earliest and the most flexible AM technologies that can process ceramics, metals, composites, and polymers. PBF was firstly developed and introduced at the University of Texas at Austin, the USA, and selective laser sintering (SLS) was the first introduced commercialised technique of this process. The rest of the PBF processes modify this basic principle of SLS in one or more manners to enable various materials to be processed, to enhance machine productivity and improve the overall efficiency of PBF technology [4]. Anisotropy [5] and stiffness [6] of the PBF process are two important factors that need to be considered in AM productions. To solve these issues, a hybrid method [7] can effectively improve the quality of the printed components. The feedstock for PBF, as named, is a powder of the material, and the quality of the parts produced is a function of various powder properties [8]. Much research is being undertaken on understanding powder behaviour. The number of machine variants for fusing powders using the laser as a heat or energy source is large, while for an electron beam, Arcam is one of the small number of manufacturers of electron beam powder bed fusion 3D printers. In PBF, a common and active area of interest has been developed based on lasers. Laser-based powder bed fusion (LB-PBF) is a favourable area across various industries such as automotive, aerospace and medical [9].

The electron beam powder bed fusion (EB-PBF) system uses an electron beam as the heat source. The electron beam passes through a series of magnetic lenses with sufficient agility to maintain multiple meltpools concurrently. To improve the efficiency of the process, the electron beam energy source uses a high vacuum within the system before the operation. It is relatively time-consuming to maintain this vacuum (compared to shielding gas environments in LB-PBF), but once established, it allows multiple technical advantages. One advantage is that the powder bed can be preheated by rastering the electron beam over the build area because gas flow losses are minimised. The bed is largely contained in a steel chamber with a heat shield for controlling the radiant heat, and there is some thermal conduction to the substrate cooling the meltpools without over-oxidising the material.

Jiang et al. [10] reviewed the manufacturability of copper produced by different AM technologies such as LB-PBF, EB-PBF and binder jetting. They reviewed the performance of these technologies over each other and discussed the advantage and challenges of each technique in the processing of pure copper components. The copper alloy has excellent mechanical and physical properties such as electrical and thermal conductivity of (58e6 S/m and 400 W/m.k, respectively), which shows that this alloy can potentially have a wide range of applications in different industries. However, the physical property of pure copper is significantly affected by impurities [11]. Pure copper also has high machinability compared to nickel, titanium and steel, so it can be widely used in aerospace, automotive and electric industries. Pure copper is the best option for manufacturing radiators, heat exchangers and cooling systems on account of its high thermal conductivity. However, due to the high geometrical complexity of cooling systems, such as heat exchangers, conventional manufacturing methods have some shortcomings and new technologies such as additive manufacturing is a good solution for this issue [12, 13]. Recently, copper has attracted more attention to being processed by AM technologies. Walker et al. [14] used semi-solid powder bed fusion systems (selective laser sintering (SLS)) to study the microstructure and mechanical properties of pure copper. They used homogenisation treatment and found that the mechanical properties and microstructure of printed copper components are comparable to other conventional manufacturing processes. Zhong et al. [15] used a laser in DED to produce copper components and found that the nano-precipitation phase was formed due to the unprotected gas environment. This precipitation phase has nano size and improves the strength of the printed parts by sacrificing ductility. Raab et al. [16] investigated EB-PBF of pure copper components. The thermal and electrical conductivity were tested, and the results they shared showed that impurities significantly affect properties. In order to improve the mechanical properties of printed copper parts, various post-treatments such as mass finishing and thermal treatment have been suggested in the literature [17].

In the processing of pure copper by AM technologies, several pieces of literature are available using LB-PBF and DED, but no comprehensive report can be found on the EB-PBF of pure copper. Therefore, this paper aims to compare the LB-PBF and EB-PBF and discuss the advantages of the EB-PBF in processing copper components. The review paper discusses the effect of printing conditions, process parameters, pre-and post-processing as well as oxygen contamination on the microstructure, mechanical properties and quality of printed parts. The paper also reviews the printing condition of pure copper using EB-PBF and introduces the challenges of producing copper components using this method.

2 Principle of EB-PBF

The electron beam can be used for both additive and subtractive-based manufacturing. For instance, this process can be used to formulate channel structures for copper ingots by melting and

Table 1 Differences between EB-PBF and LB-PBF [19]

Characteristic	EB-PBF	LB-PBF
Thermal source	Electron beam	Laser
Production rate	3 kg/h	0.2 kg/h
Atmosphere	Vacuum	Inert gas
Scanning	Deflection coils	Galvanometers
Energy absorption	Conductivity-limited	Absorptivity-limited
Powder preheating	Use electron beam	Use infrared or resistive heaters
Scan speeds	Very fast, magnetically driven	Limited by galvanometer inertia
Energy costs	Moderate	High
Surface finish	Moderate to poor	Excellent to moderate
Feature resolution	Moderate	Excellent
Materials	Metals (conductors)	Polymers, metals and ceramics
Powder particle size	Medium	Fine

evaporation [18]. If the electron beam is used in subtractive regions, it is called electron beam machining, which is not within the scope of this research.

Electron beam powder bed fusion (EB-PBF), which is known as selective electron beam melting (SEBM) and electron beam melting (EBM) by Arcam, has become a successful method for PBF. EB-PBF system uses a high-energy electron beam (compared to laser-based powder bed fusion (LB-PBF) to fuse metal powder particles. Researchers at the Chalmers University of Technology, Sweden, first developed this process. EB-PBF was commercialised by Arcam AB, Sweden, in 2001, and is now owned by GE.

Similar to LB-PBF, in the EB-PBF, a focused electron beam scans along a thin layer of spread and settled powder, causing localised fusion/melting and solidification per the slice cross-section. Table 1 summarises the differences between EB-PBF and LB-PBF. Most of the presented differences in this table are due to EB-PBF having an energy/heat source of electrons. Nevertheless, other differences are associated with engineering trade-offs as practised in EB-PBF and LB-PBF and are not necessarily inherent to the processing.

In LB-PBF, laser beams heat the powder bed when powder particles absorb the photons, while in EB-PBF, by transferring kinetic energy from incoming electrons into powder particles, the heating process is carried out. When powder particles absorb electrons, they gain an increasingly negative charge that causes two possibly detrimental effects: (I) If the repulsive force of neighbouring negatively charged particles overcomes the frictional and gravitational forces holding them in place, there will be a rapid expulsion of powder particles from the powder bed. This causes it to produce a powder cloud (that is more harmful to fine powders than coarser powders); and (II) increasing negative charges in the powder particles will tend to repel the incoming negatively charged electrons, consequently generating a more diffused beam. There are no such complimentary phenomena

with photons; thus, the conductivity of the powder bed in EB-PBF must be high enough that powder particles do not become highly negatively charged. The scan strategies help to avoid the build-up of regions of negatively charged particles. In reality, the electron beam energy is more penetrative and diffused, in the powder, so as not to build up too great a negative charge in any one location. This causes the effective meltpool size to increase, producing a larger heat-affected zone. Therefore, the minimum feature size, layer thickness, average powder particle size, resolution and surface quality of an EB-PBF process are typically larger than for a laser-based process. As discussed, in EB-PBF, the powder bed must be conductive; therefore, EB-PBF can only be used to process conductive materials (e.g., metals), while lasers can be applied to the material that can absorb laser energy (e.g., metals, polymers and ceramics) [9]. The limitation in laser processing additive manufacturing is the amount of absorption. For instance, LB-PBF is not effective for materials with a low absorption ratio such as aluminium (absorption ratio of 9%). Figure 1 shows the schematics of EB-PBF.

3 EB-PBF of copper

Pure copper has excellent mechanical and physical properties, including high thermal conductivity (400 W/(m·K)), electrical conductivity (58×10^6 S/m) and corrosion resistance properties. These make pure copper the ideal material for electronic industries and a suitable candidate for the production of heat exchangers and other cooling parts [20–22]. Copper has various alloys, and the best-known traditional types are bronze, where tin is a significant addition, and brass, using zinc instead. Both bronze and brass are imprecise terms, having both been commonly referred to as "lattens" in the past. There are as many as 400 different copper and copper alloy compositions that have been classified such as copper, high copper alloy, brasses, bronzes,
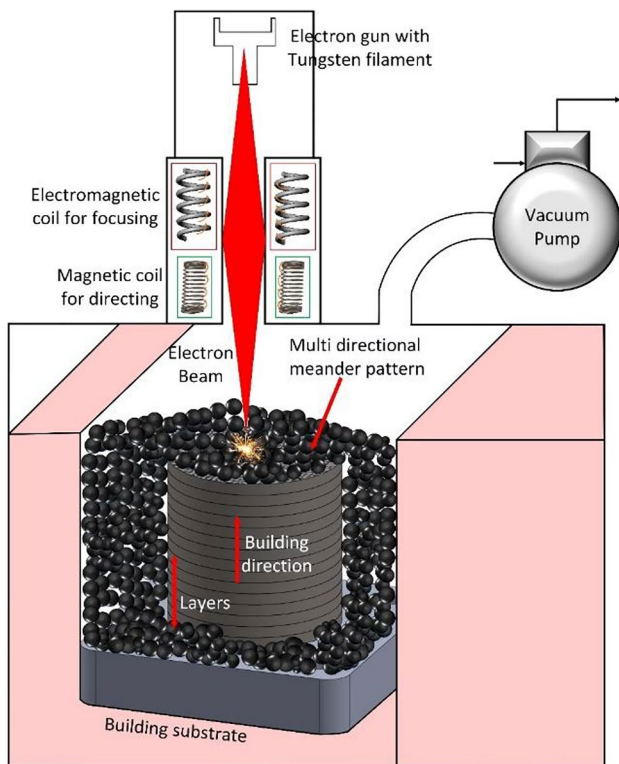
Fig. 1 Schematics of an electron beam powder bed fusion process [19]

copper nickels, copper–nickel-zinc (nickel silver), leaded copper and special alloys which are listed in Table A1 [1, 2, 23]. Pure copper – due to its high thermal conductivity, electrical conductivity and machinability – is widely used in automotive, aerospace and electric fields [24]. In particular, pure copper due to its high thermal conductivity and cost-effectiveness is the main raw material for heat exchangers and radiators [25]. With the rapid development of the manufacturing industry and the electrical industry, the requirements for manufacturability including surface quality and geometrical complexity of copper productions have gradually increased. The conventional production methods are difficult to realise the processing of complex structures [26], which necessitates new manufacturing methods such as additive manufacturing to process the copper alloys.

The influence of process parameters on the quality of copper in electron beam melting is also used for refining the microstructure and mechanical properties of the Cu components. For instance, Vasilyeva and Vutova [27] have used an electron beam for refining copper alloy from the impurities such as Sb, Pb and Sn. By developing and innovating thermal management, the production of complex copper parts has been put on the agenda and has attracted a lot of attention.

4 Discussion

The microstructure and mechanical properties of EB-PBF of copper are discussed in this section to show how the process affects these properties and the quality of as-built components. Moreover, the effect of post-processing such as thermal treatment on the quality of the printed copper component is discussed in this section to reveal how the quality of the production can be improved.

4.1 Microstructure and mechanical property of EB-PBF copper components

The production of pure copper components by EB-PBF shows less chance of oxides as the material is processed in a vacuum. High preheats in EB-PBF show less thermal gradient and internal stresses in cooling. Ramirez et al. [28] investigated the microstructure and mechanical properties of open cellular parts. They showed that EB-PBF is a great tool to produce lattice copper parts, such as heat exchangers. This study showed that Cu_2O appeared in the microstructure and it can improve the mechanical properties. However, if the Cu_2O exceeds a certain value (0.0235%wt), cracks happen, which negatively affect the mechanical properties.

Pure copper powder is much less reflective (< 50%) to the electron beam compared to the laser beam (~ 70%), and this causes higher induced heat on the surface of the powder bed. The generation of fully melted tracks and a reduction in pore formation were observed. However, due to difficulties such as over sintering due to increased heat in the build area, a higher layer cooling time was introduced to maintain the temperature of the process, which leads to elemental segregation and related defects. Momeni [29] reported that chrome-rich spheres ($1 \leq \mu m$) surrounded by Cu matrix are formed in EB-PBF of copper chrome parts. This study also reported that elemental segregation can produce heterogeneous nucleation of primary Cr-rich particles and affect the produced parts.

Guschlbauer [30] studied the effect of oxygen content in EB-PBF of copper when preheat was 530 ℃. Results of this research showed that the powder with high oxygen level (0.0235%wt) has cracks, whereas samples from the powder with low oxygen content are crack-free. The study showed that for a high amount of oxygen content when the scan speed was selected below 1000 mm/s, cracks appear and for scan speed of 1000–1500 mm/s, samples are not produced due to Rayleigh instability. The best condition for printing copper components was found at a scan speed of 500 mm/s and power of 450 W. The mechanical properties of the crack-free parts were studied and compared to annealed and wrought copper. The related phenomena

for each crack are also investigated and discussed in this paper.

Lodes et al. [31] reported that the governing factor in the EB-PBF of copper is the cooling rate. They reported that low process temperature should be used when printing larger copper components. A hydrogen furnace process of the pure copper for EB-PBF was studied by Ledford et al. [11]. The authors examined three types of powder with different oxygen content. When the hydrogen furnace process is applied to the powder, part of the oxygen is used. Hydrogen heat-treated copper powder was used to overcome the oxidation of powder feedstock and subsequent issues. This treatment showed that the oxygen content of 50 wt ppm with minimal residue hydrogen content (less than 5%wt) led to the complete removal of trapped H_2O vapour from the printed parts and heat-affected zone. This research also revealed that hydrogen heat treatment reduces the amount of oxygen and related issues. As shown in Fig. 2, treated samples appeared to have some cracks in the powder particles which is attributed to the escaping of the H_2O vapours. This causes the interconnected porosity along the grain boundaries beneath the powder surface, which leads to additional porosity and can have an effect on the mechanical properties.

Hot cracks need a solidification range to form a persistent liquid film in between the grain boundary, which is driven by a cellular or dendritic melt front [32]. Coarse oxide particles at the fracture surface are an indicator of the hot crack mechanism formed during the solidification of the persistent liquid film. This investigation also showed another type of cracking named "ductility dip cracking (DDC)" that appears after solidification. The mechanism of forming DDC is based on the ductility dip, a brittle behaviour of face-centred cubic (FCC) metals at elevated temperatures [33]. In the cooling procedure due to material shrinkage, the grain boundaries are shearing and sliding apart (similar to creep). Indicative of this mechanism is a smooth wavy crack surface and fine-distributed Cu_2O particles in the copper matrix [32]. This research showed that the role of the oxides at the fracture surface is unclear. If the oxides do not pin the grain boundaries, the crack can grow easier. The oxygen increases the embrittlement of the copper, and to avoid crack formation, a powder with a low oxygen level was recommended. Additionally, a high scan speed in the process suppresses the crack development. So, the oxygen level of the powder has to be strictly controlled to prevent the crack formation of pure copper in EB-PBF.

Fig. 2 Scanning electron micrograph of an HO-Cu particle after hydrogen treatment, before (**a**) and after (**b–d**) in situ SEM heating on a SiC chip to 400 ℃ at 100 ℃/s under a vacuum [11]. (No permission number is required to reuse all or part of an article published by MDPI)
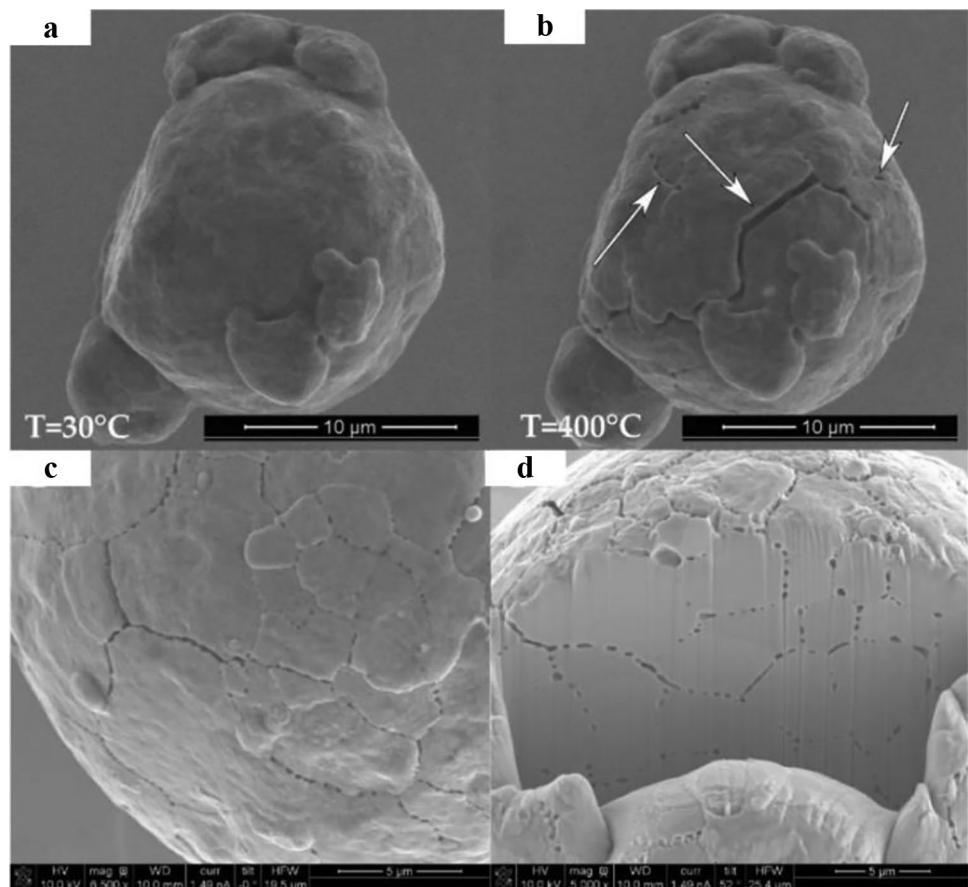
Lodes et al. [31] worked on finding the process window for the generation of dense copper parts. They used raw material for this process which was gas atomised 99.94% pure copper powder with an average particle size of 45–106 μm. The build process was carried out by the Arcam A2 EBM machine. The microstructure and porosity were analysed parallel to the build direction on five microsections. This research showed that pure copper printing at lower preheating build temperatures has to be used due to the high sintering tendency of the powder compared to titanium. This can be related to the high thermal conductivity of pure copper. The research showed that the high thermal conductivity causes problems with heating, and a high tendency to sinter pure copper can result in problems of powder sticking during raking. Therefore, the process parameters should be set in such a way as to produce lower temperature on the surface of the meltpool. Also, the results of this research showed that the porosity has no strong relation to the scan speed for the examined process parameters. For a successful build, it was suggested to produce the copper samples with speed and beam current of 3000 mm/s and 15 mA, respectively. Figure 3 shows the porous and dense copper components which were obtained by changing energy density.

The results showed that physical density is a direct function of energy density. The best relative density of 99.5% was reached at a line energy density of 0.275 J/mm. Samples produced at low energy density (Fig. 3 left) has more porosity because some regions were not completely melted. This is related to lower induced energy density and temperature of the meltpool and subsequently higher surface tension. As a result, inferior wetting occurs and the meltpool cannot cover all areas leading to the formation of the pores. The samples presented in Fig. 3 (right) have too much energy density leading to swelling. Due to the overheating of the sample, copper particles may stick to the meltpool during raking, resulting in porous areas and binding defects. Similar results were found on TiAl6V4 produced by EB-PBF [34]. The best operational or preheat temperature for copper printing was reported in a range of 400 ± 10 ℃. This preheat minimises the temperature differences of the build plate and meltpool and reduces the residual stresses due to periodic heating and cooling in EB-PBF.

Raab et al. [16] investigated the physical properties of pure copper (99.91%) produced by EB-PBF. Laser flash analyses and eddy current measurements were used to find the thermal and electrical conductivity of printed products. The relation between conductivities and porosity found that

Fig. 3 Micro- and photographs of cube-shaped EB-PBF samples built with different line energies. The sample with 0.15 J/mm linear energy density (left images) has common pores with lots of binding defects. The sample with 0.3 J/mm energy density (centre column images) has a high energy density. The sample with 0.35 J/mm (right images) shows swelling and powder sticking because of too high energy input, though the micrograph shows some degree of porosity again [31]. (Elsevier permission No: 5300060964327)
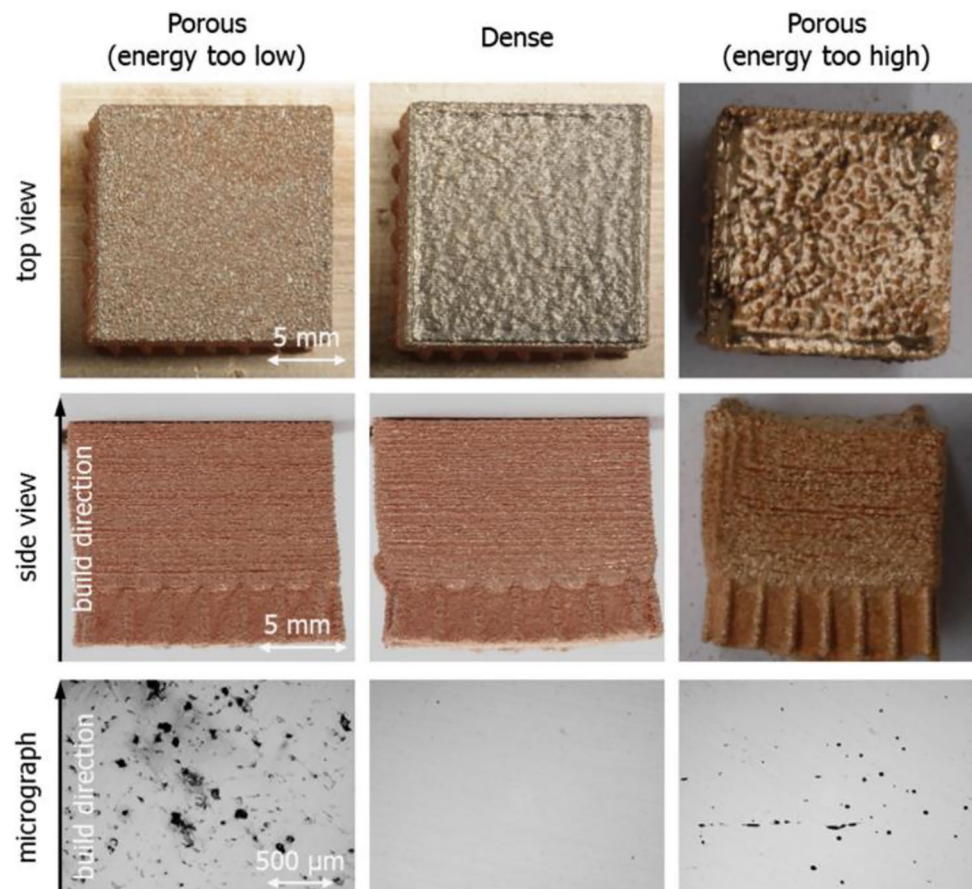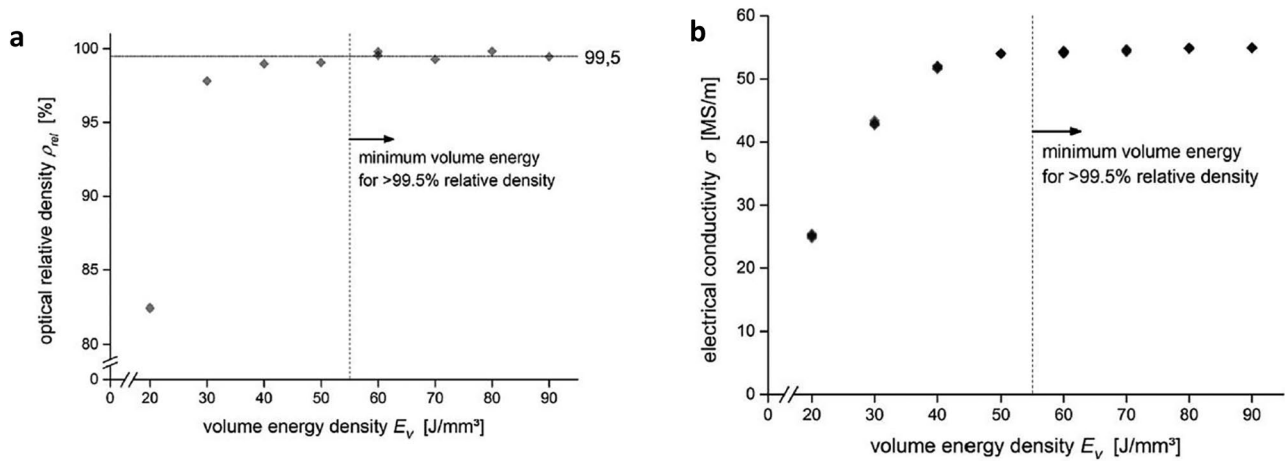
Fig. 4 **a**, **b** Relative density and electrical conductivity of EB-PBF copper components produced with different volume energy densities. (John Wiley permission No: 5340061151075) [16]

99.95% of dense specimens with nearly optimal conductivities ($\sigma = 55.82$ MS/m and $\lambda = 400.1$ W/(m.K)) can be fabricated with this production process. Results also showed that the samples with low porosity have the highest electrical conductivities, while for samples with high porosity, electrical conductivities were low.

Figure 4a shows that samples that were produced by the energy density of 40 J/mm^3 or above have higher than 99.5% relative density. Figure 4b shows that the printed components with higher than 50 J/mm^3 energy density have 55.28 MS/m electrical conductivity, which is equal to 96.2% IACS.[1] Definition of 58 MS/m shows 100% conductivity. The authors reported that the small deviation from the theoretical maximum conductivity of copper (59.7 MS/m) can be explained by the characteristics of chemical impurities. In addition, pores reduce the conductivity due to a reduction in conduction cross-section and electron transformation.

Pobel et al. [26] added 5% Al_2O_3 to copper- and investigated the meso- and micro-scale structures of EB-PBF parts by analysing the optical microscopy (OM) and scanning electron microscopy (SEM) as well as using energy dispersive X-ray analyses (EDX). This research has shown that Al_2O_3 was partly melted and separated from Cu and that caused heavy demixing and lots of dispersion strengthening. Both separation and agglomerations of dispersed particles that were found in this research are associated with too much energy input and the high temperature of the meltpool. This research also showed that lower packing density leads to a higher difference in density that gets more pronounced with the next subsequent layers. The high porosity ranging from 2 to 20% can be related to phase separation and meltpool

dynamics features. The microstructural characterisation of 5% Al_2O_3 and pure copper showed three phases consisting of (A) pure copper, (B) both Cu and Al along with oxygen indicated dispersed ceramic particles within the Cu matrix, producing a zone with a marmorate appearance and (C) solely alumina, which can be seen in Fig. 5. The latter phase that includes alumina-rich portions from a network has a high tendency to form and incorporate defects and produces a highly irregular surface.

Frigola et al. [35] processed copper material by EB-PBF using three different powders with an average size of 55 µm to find a proper process window to produce fully dense components. They used two types of powder produced by atomisation in argon and the third atomised in air. The authors of this research mentioned that the processing of copper using electron beam powder fusion is challenging due to high thermal conductivity. This feature of the copper highly conducts heat away from the melt area, resulting in a local thermal gradient and subsequently producing some issues like delamination, curling and ultimately part failure. The delamination happens because the copper cools down very fast, and this increases the surface tension and reduces the wetting and intra-layer adhesion. Moreover, the high ductility of copper hinders post-build powder removal and recovery, and particles tend to agglomerate reducing overall flowability which negatively affects the morphology of the meltpool tracks and subsequently of the printing process.

Figure 6a shows a mixture of high oxide powder type C and powder type A which shows the columnar oxide and needle shape microstructure along with build direction. Figure 6b shows the columnar grain structure which is mixed with oxide when powder type B was used. Figure 6c shows that the microstructure in EB-PBF is highly driven by the size of the sample. For instance, this figure shows that using

---

[1] IACS is International Annealed Copper Standard.

Fig. 5 The EDX spectrum of the primary phase (1) reveals pure copper, while the marmorate zones (2) contain both Cu and Al along with O which indicates dispersed ceramic particles within a Cu matrix. The secondary phase (3) shows no presence of copper and consists solely of alumina (Wiley permission No: 5343430184126) [26]
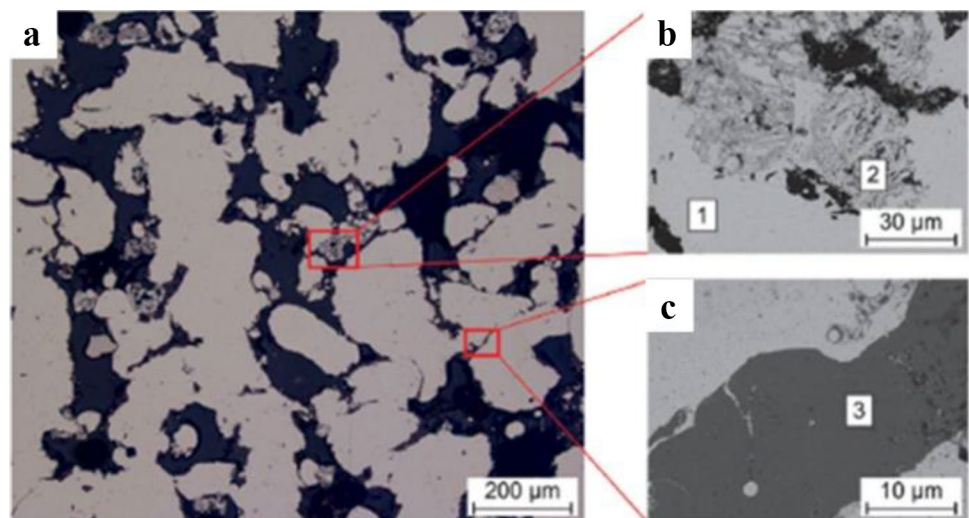
a smaller sample (Fig. 6c) must generate a higher temperature as an equiaxed microstructure was obtained, which is similar to the wrought copper microstructure. This research has shown that different factors such as packing density as well contact area between powder particles have a significant influence on thermal conductivity and flowability of the powder. Results of this research showed that the oxygen content in the powder plays an important role in the process.

Cheng and Chou [36] numerically studied the various materials, such as Ti-6Al-4 V (Ti64), IN718, AISI316L, TiAlNb and copper (Cu) using finite element modelling to simulate the thermal behaviour of the process. They used the design-of-experiment approach and statistical analysis such as analysis of variance (ANOVA) to evaluate the characteristics of meltpool shapes for different process conditions. The effect of specific material properties on the
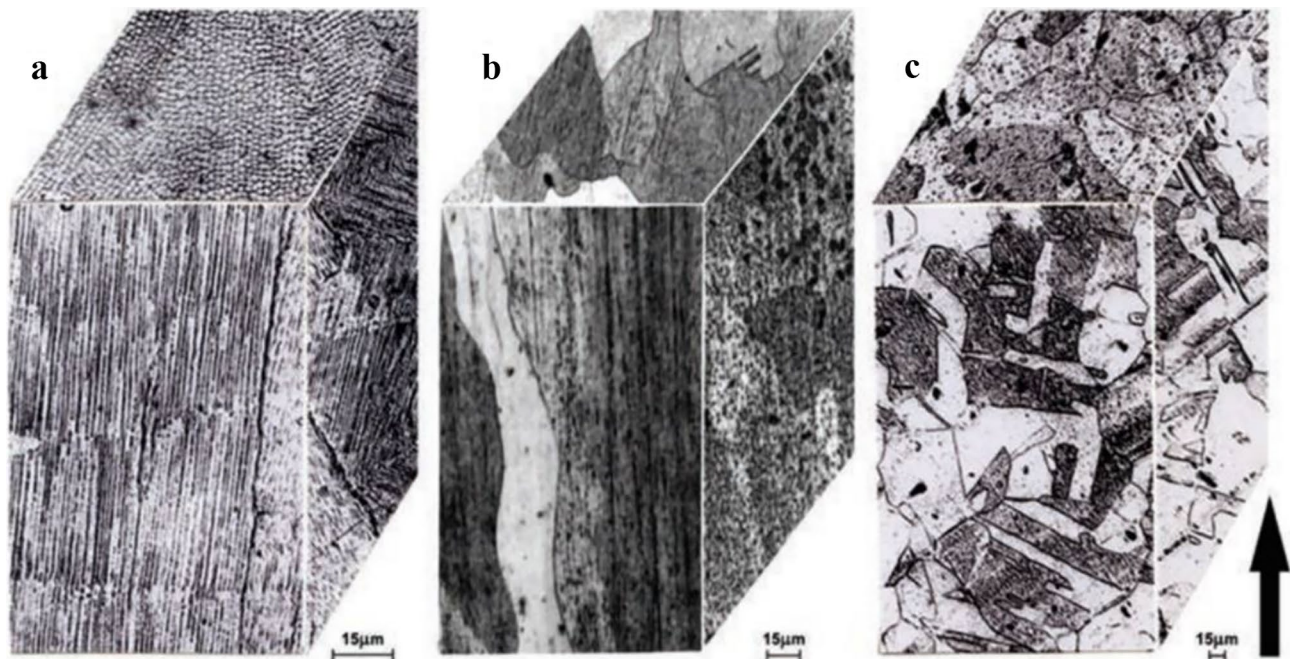

Fig. 6 3D construction demonstrates the microstructure of copper components by EB-PBF, **a** from a mixture of 99.80% Cu powder type C and a prior, high oxide powder type A, **b** 99.99% Cu powder type B and **c** 99.99% Cu powder type B built at elevated temperature. The build direction is shown by the arrow. (No permission number is required to reuse the materials from open access publications that are published by ASM International) [35]
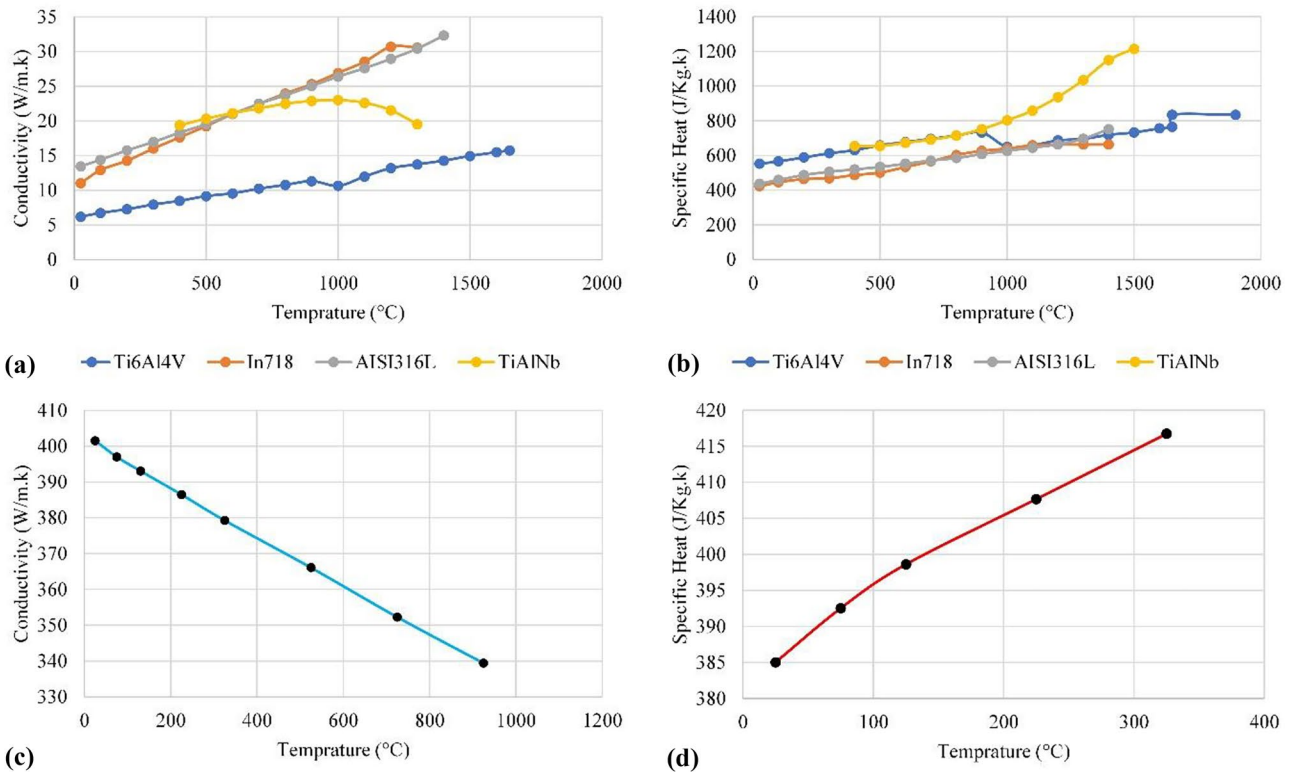
Fig. 7 Thermal properties of studied materials: **a** thermal conductivity, **b** specific heat, **c** thermal conductivity of Cu and **d** specific heat of Cu [36–38]

meltpool morphology was studied based on the physical properties. The authors used a thermal model to evaluate material thermal property effects such as specific heat, conductivity, latent heat of fusion and melting temperature on the meltpool morphology including length and width. The numerical simulation has been carried out by Abaqus software, treating the powder and substrate as connected solid elements with the same material properties except for powder exhibiting reduced conductivity. Radiation at the powder surface was considered, but the model excluded meltpool convection. The main outcomes showed that the melting point of the material is the most important driving factor for meltpool morphology and size. The role of the material thermal conductivity can outweigh the melting point and drive the meltpool size. Variation of temperature versus conductivity and specific heat for different materials versus copper is shown in Fig. 7. This figure shows that the thermal conductivity of the copper is reducing versus increasing the temperature; however, in the elevated temperature ranging from 800 to 1000 ℃, the value of conductivity for copper is still about 10 times more than the studied materials presented in Fig. 7, which shows how challenging copper processing by EB-PBF can be. It is demonstrated that at the same meltpool temperature, the meltpool size commonly reduces with the increase in

conductivity-specific heat and latent heat of fusion. For the investigated materials in this study, low melting temperature commonly produces a large meltpool size. Also, a high conductivity greatly reduces the meltpool dimension including length and width. In addition, specific heat and latent heat of fusion were introduced as two significant factors that can derive the meltpool size. The specific heat determines how fast the processed material will respond to the interaction of heat flux and the latent heat of fusion determines how easily the material can be changed from one side of the melting temperature to the other.

The static tensile properties of unalloyed copper produced by EB-PBF were studied by Tarafder et al. [39]. The test samples in this study were produced by nitrogen gas atomised copper powder with a particle range of 45–106 μm. The samples were divided into three different conditions including as-fabricated, hot isostatic pressing (HIP) and vacuum annealing in both perpendicular and parallel to build direction. Mechanical properties including ultimate tensile strength (UTS), yield strength, elongation and microhardness were evaluated (Fig. 8).

The overall outcomes of this study have shown that different post-processing can improve mechanical properties. For instance, HIP slightly improved sample density from 8.91 to 8.94 g.cm^{-3}, while vacuum annealing reduced the
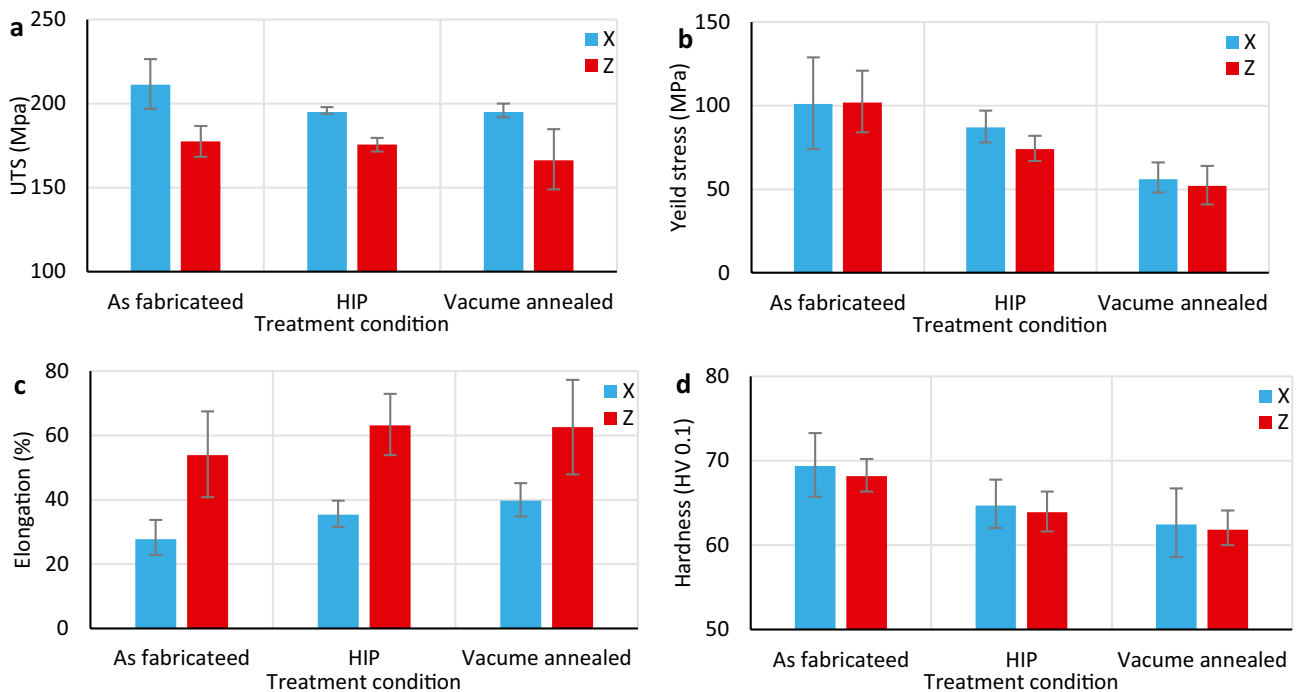
Fig. 8 Mechanical properties of **a** ultimate tensile strength, **b** yield strength, **c** elongation to failure and **d** Vickers microhardness. Error bars indicate a 95% confidence interval based on the pooled variance of all samples [39]

oxygen content from 450 to 275 wt. ppm. The authors reported that ANOVA analysis on the determining factors on the value of mechanical properties in this research and the smallest P values were found ($P > 0.15$). Samples printed in the X-direction were found to have higher ultimate tensile strengths compared to the samples printed in the Z direction. This research shows that as-built components have the highest yield strength, while post-processing including HIP and vacuum treatment leads to decreased strength but improved ductility and elongation. In pure metals and alloys processed by EB-PBF, various factors influence strength and elongation in specimens showing columnar grains and crystallographic anisotropy, which complicate the interpretation of the results. Factors such as porosity, oxidation, precipitation or allotropic phase changes, layer-induced defects, residual stress and localised cracking, among others, can have a significant impact on the results of the mechanical tests.

To explore the influence of crystallographic texture of EB-PBF of Cu parts, EBSD has been performed as shown in Fig. 9. The reconstructed EBSD IPF maps in Fig. 9 demonstrate columnar grains and a mix of crystallographic orientations for all as-built vacuum-annealed and HIP samples. As can be seen in this figure, the microstructure of the as-built samples was found to be slightly smaller than heat-treated test samples. The intention of these treatments was to

improve the breaking elongation, while UTS, yield strength and microhardness were reduced. Results also showed when the density of the samples reaches almost the theoretical values, the observed differences in ultimate tensile stress and ductility are proposed to be controlled by orientation anisotropy and interdependencies between the grain morphology and dislocation movement. Since this heat treatment significantly changes the residual stress, the yield strength for the as-built and thermal-treated samples has significant changes.

Ramirez et al. [40] investigated a precipitate-microstructural architecture developed in the fabrication of solid copper parts processed by EB-PBF using powder particle sizes 50–60 μm. The high density of Cu_2O precipitates showed an interesting example of a precipitate-dislocation architecture. Such architectures were observed by scanning and transmission electron microscopy and optical metallography. The Cu_2O precipitate was retained in the process and distributed in special architecture along with layer heating and cooling.

They observed equiaxed precipitate-dislocation cell-like arrays ranging 1–3 μm in the X-direction perpendicular to the build direction with elongated or columnar-like arrays ranging from 12 to > 60 μm in length and corresponding spatial dimensions of 1–3 μm. The investigation showed that the hardness for such architectures raised to 83–88 HV, while the pure EB-PBF copper with 99.99% purity has 72 HV and
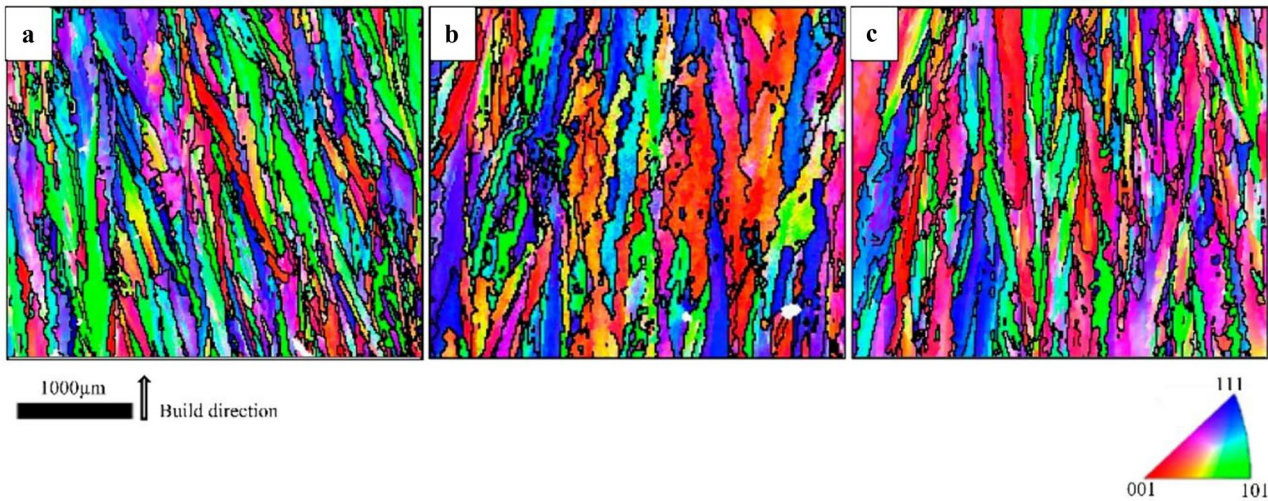
Fig. 9 Inverse pole figure maps of the as-fabricated, HIP and vacuum-annealed specimens along the build direction shown with an arrow alongside the scale bar (**A**–**C**) [39]. (No permission number is required to reuse all or part of an article published by MDPI)

conventional pure copper's hardness is 57 HV. The observation showed the prospect of controlling the microstructure and subsequently mechanical properties via controlling the level of oxygen. The large columnar grains observed in Fig. 10b appear to grow in the column section to 1 cm in height with some degrees of epitaxial growth from the substrate.

This research showed that the grain structure is not significantly changed from the substrate and there is clear evidence of oxygen precipitate segregation at the grain and grain boundaries, especially the high energy grain boundary and high angle grains. In this condition, almost no cracking is formed along the straight observation direction, which causes coherent twin boundaries that in copper
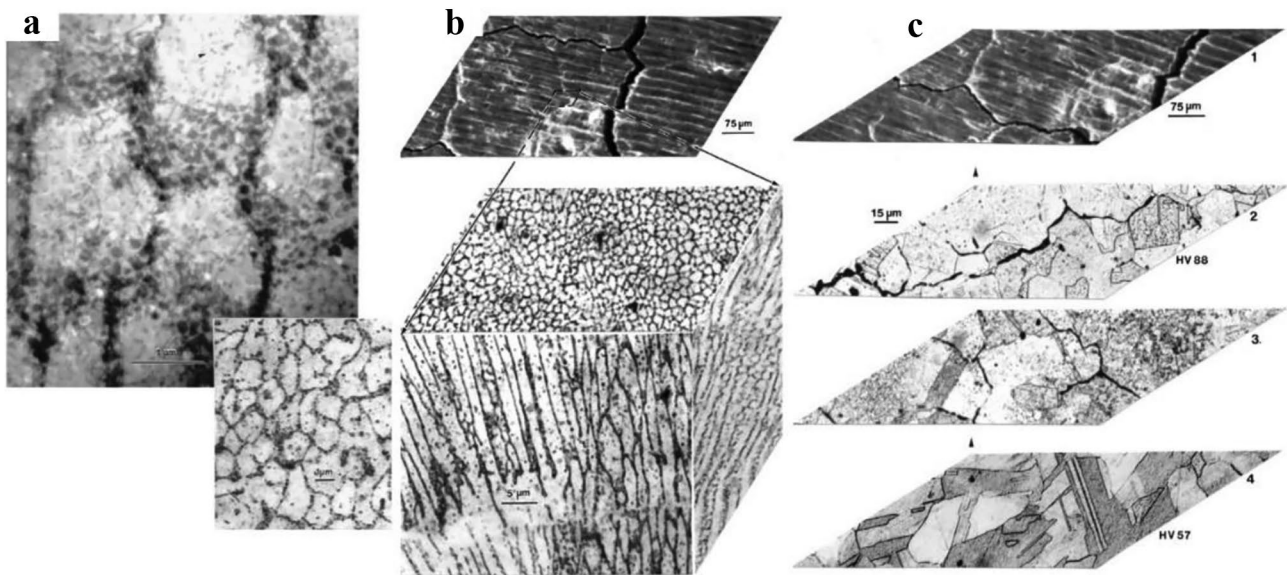

Fig. 10 a TEM bright-field image showing precipitate-dislocation arrays corresponding to the horizontal reference plane. **b** Spatial composite illustrating a typical horizontal reference plane section in an intergranular-like domain along with 3-D image composite for the EB-PBF component. **c** Spatial array illustrating the surface structure of the EB-PBF component (1) to the upper base plate microstructure/ grain structure (2 and 3) and the bottom of the plate (4). The related micro indentation hardness averages in Vickers are also indicated [40]. (Elsevier permission No: 5300100993994).

have significantly less interfacial free energy compared to nominal grain boundary free energy. Therefore, the hardness between the substrate and the top was shown to have about 53% differences. The substrate also showed it was 26% softer than precursor powder (in the middle or core of the printed components). This observation proved that precipitation-related hardening happens in EB-PBF of copper which is shown in Fig. 10c.

Ledford et al. [41] studied the EB-PBF of high purity copper for overhang structures with powder particle sizes ranging from 10 to 50 μm. The authors performed DoE and produced 9 samples with different speeds, thicknesses and running points to detect the defects in situ the EB-PBF process by backscatter monitoring. The defects were classified as porosity, cracks or lack of fusion. This monitoring system showed two direct advantages in EB-PBF. First, as the component sizes become bigger, or use higher density metals (e.g., copper, nickel), traditional non-destructive evaluation techniques will lack the resolution to find the defects. This becomes an issue when complicated geometry is desired. The presented in-situ monitoring system in this research showed the ability to detect defects and correlate them to the process window, which is required for successful printing jobs. The second advantage of this monitoring system is the real-time nature providing unique opportunities for in-situ control strategies that are difficult to perform using image-based monitoring techniques such as infrared (IR) or near IR.

Figure 11 shows the variation in the samples taken from the solid regions or core of the parts (without overhangs)

resulting from changes in beam speed due to the changes in the turning points function. The feasible space for fully dense material measured from the overhang region (that has much lower thermal conductivity) is shifted drastically to the right-hand side of the processing windows and corresponds to a low volumetric energy density. This diagram explicitly describes the required changes in localised energy density necessary to produce fully dense material in the overhanging regions with drastically different thermal boundary conditions.

The effect of different scanning pattern approaches during EB-PBF production of waveguides was investigated by Lomakin and his team [42]. Two different scan patterns were used to produce waveguides and attenuation checks. As can be seen in Fig. 12, the hatch pattern produces irregular and blurry edges due to high meltpool temperature as a result of the short time difference between the two tracks. The second pattern is contoured, which showed less effect on the attenuation. This identifies that the contour pattern is the better tool for producing electronic devices by EB-PBF for signal transmission purposes.

The EB-PBF of the mixture of copper and chrome (Cu-25Cr) has been examined by Momeni et al. [29]. Since the temperature of chrome is largely higher than copper, the high energy density was used to obtain a fully melting condition which produced too high local temperature in the meltpool. The microstructure analysis showed that fine microstructure consisting of Cu-25Cr was obtained. This analysis showed that Cu and Cr are quite distinguishable, and the formation of a fine nodular Cr-rich phase showed that liquid phase separation happens during

Fig. 11 EB-PBF processing space (volumetric energy density) for pure copper as a function of beam power [11]
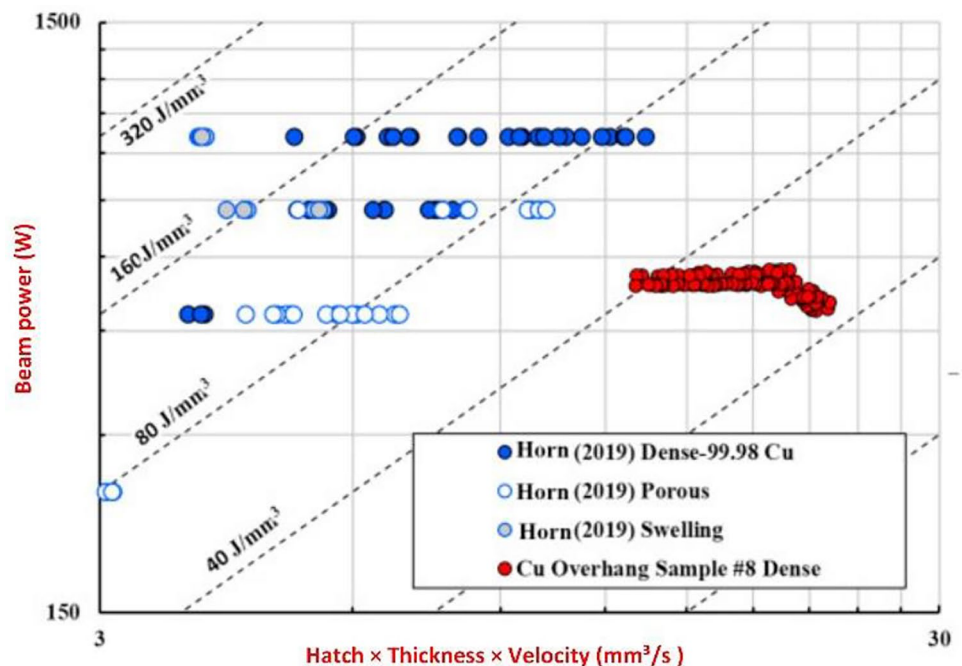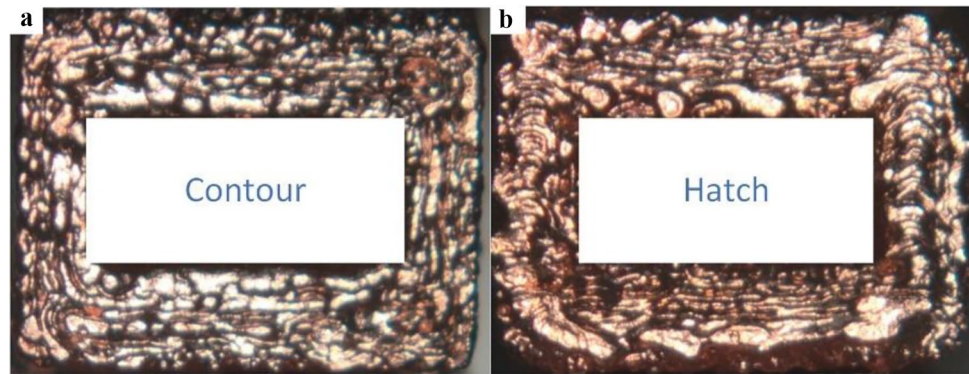
Fig. 12 Resulting waveguide cross-section of the contour (left) and hatch (right) processing pattern on the topmost printed layer [42]

the solidification. This microstructure that is shown in Fig. 13 is a result of a uniform distribution of fine Cr-rich spheroids (< 1 μm) that are entrapped by the Cu matrix. The fast-cooling rate in EB-PBF followed by spinodal decomposition is another reason for entrapping Cu particles in the Cr phase.

Ramirez and his team [28] studied Cu reticulated mesh and stochastic open cellular foams processed by EB-PBF. Mechanical properties including Young's modulus versus density and relative stiffness versus relative density were investigated and compared with the Gibson-Ashby model for open cellular foams.

They used precursor Cu powder containing Cu_2O precipitates and fabricated parts with arrays of Cu_2O precipitates and interconnected dislocations microstructure. These were shown to have a hardness of about 75% above conventional Cu components. The Cu_2O precipitates and additional precipitates from the EB-PBF process formed a microstructural array that causes hardening and improves the strengthening of mesh struts and foam ligaments. Figure 14 shows a TEM bright-field image for horizontal plane and solid test case identifying Cu_2O precipitate and dislocation cell-like microstructure. Dislocation intermixed with the Cu_2O precipitates is shown with label D, and vacancy dislocation loops are

shown by label V. The illustrated dislocation in Fig. 14 drives the hardness. The measured hardness in the horizontal plane perpendicular to the build direction obtained 85HV, which is 18% higher than the hardness in vertical surfaces. The hardening occurs due to the effect of Cu_2O precipitates and increasing dislocation density. The dislocations tend to prevent the motion of atoms' planes, and more force is required to deform the material leading to improve the hardness and strength.

The hardness of the strut and foam ligament was captured and found to be higher with 164HV and 70HV, respectively, which were the same for all orientations. The hardness of the annealed and conventionally wrought Cu and heavy cold work is 55 HV and 115 HV [43], which demonstrates that the related precipitation that appeared in this study improved the hardness of all solid, foam and ligament components. This research showed that the open cellular structures printed by EB-PBF have considerable potential for intricate multi-functional electrical and thermal systems. Wen et al. [44] studied the characterisation of single contact asperity of EB-PBF of Cu-Si material by developing a numerical model. They studied the temperature and pressure of the process on thermal contact resistance (TCR). Results showed that

Fig. 13 High-resolution FIB-SEM image of EB-PBF processed Cu-25Cr alloy: **a** droplet-shaped Cr particles and/ or spheroids and **b** small Cu particle [29]. (Elsevier permission No: 5300110291668)
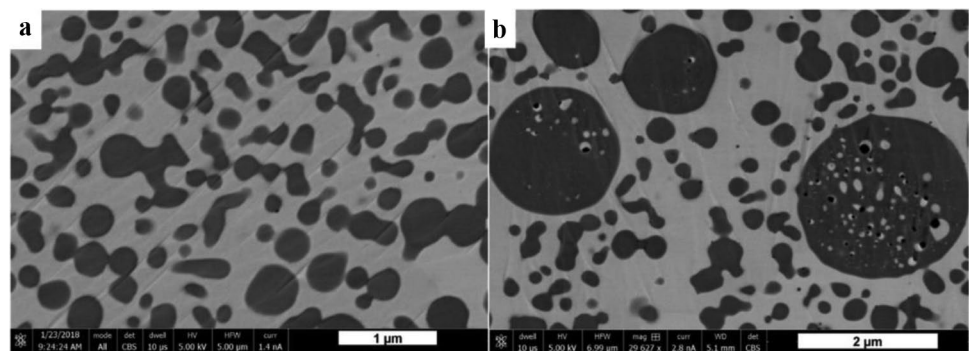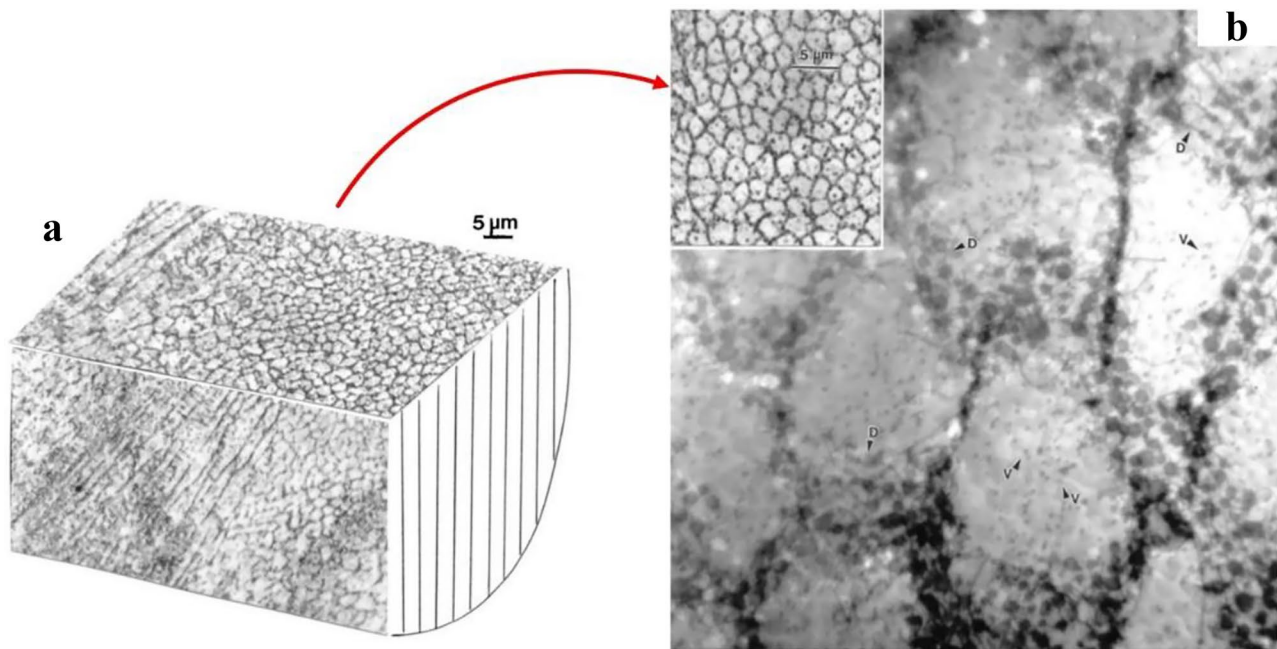
Fig. 14 TEM in the horizontal plane of Cu_2O illustrating dislocation cell-like microstructures comprising the Cu_2O precipitates and vacancy dislocation loops [28]. (Elsevier permission number: 5300110575518)

the influence of pressure on the TCR of Cu-Si is far greater than the temperature. The open cellular structure can be produced by PBF [45] which has high popularity for researchers and designers. Wolf et al. [46] investigated the open cellular Raney-Copper catalysts with high geometric complexity produced by EB-PBF. The authors studied the dealloying of Al-Cu and the microstructure of the printed components. Figure 15 shows the printed Cu-70Al catalysts using powder particle sizes of 45 to 105 μm. The authors reported that the temperature at the top of the meltpool is relatively higher than at the bottom of the substrate. Therefore, they suggested a preheating of 450 ℃ to produce a similar temperature for all areas of the meltpool. The results showed that after a partial dealloying using an aqueous NaOH solution, the printed struts exhibited a core-cell structure consisting of dense core alloy and nano-porous copper skin. The core of the material showed sufficient mechanical stability, while the skin showed a high reaction surface area that meets the standards of reactor application.

Yu et al. [47] modelled the precipitate process of Al-Cu in EB-PBF using a cellular automaton model. This model can simulate the solid-state phase transformation using a mixed mode containing both growth and decomposition.

The result of this study indicated that increasing the preheat leads to precipitate decomposition. Furthermore, the

research showed that in lower preheats, the precipitate is distributed and their size is uniform. This research showed that precipitates are more distributed at grain boundaries corners, and edges when the preheat temperature are lower.

Gamzina et al. [48] reported that electron polishing is an ideal method for post-processing of EB-PBF of copper alloys. In this research, the current resolution of EB-PBF of copper is on the order of a few 10 microns and can be improved by electron polishing by about 50%. The authors also examined the feasibility of copper printing on an alumina substrate, which was successful. This shows that the EB-PBF can print different materials on top of each other. It should be noted that the interface of different materials is a fertile ground for defects that needs more care and consideration. Table 2 shows the mechanical properties of the EB-PBF pure copper for the samples printed in fully dense conditions in different research.

4.2 Technical challenges of EB-PBF of pure copper

In EB-PBF of copper, the lack of component-level data can be related to the significant processing challenges. Even though copper has a relatively low melting temperature, several physical properties of this material present significant processing challenges for EB-PBF. The narrow

Fig. 15 The printed Cu-70Al catalysts using powder particle sizes of 45 to 105 μm [46]. (Open access no. permission is required)
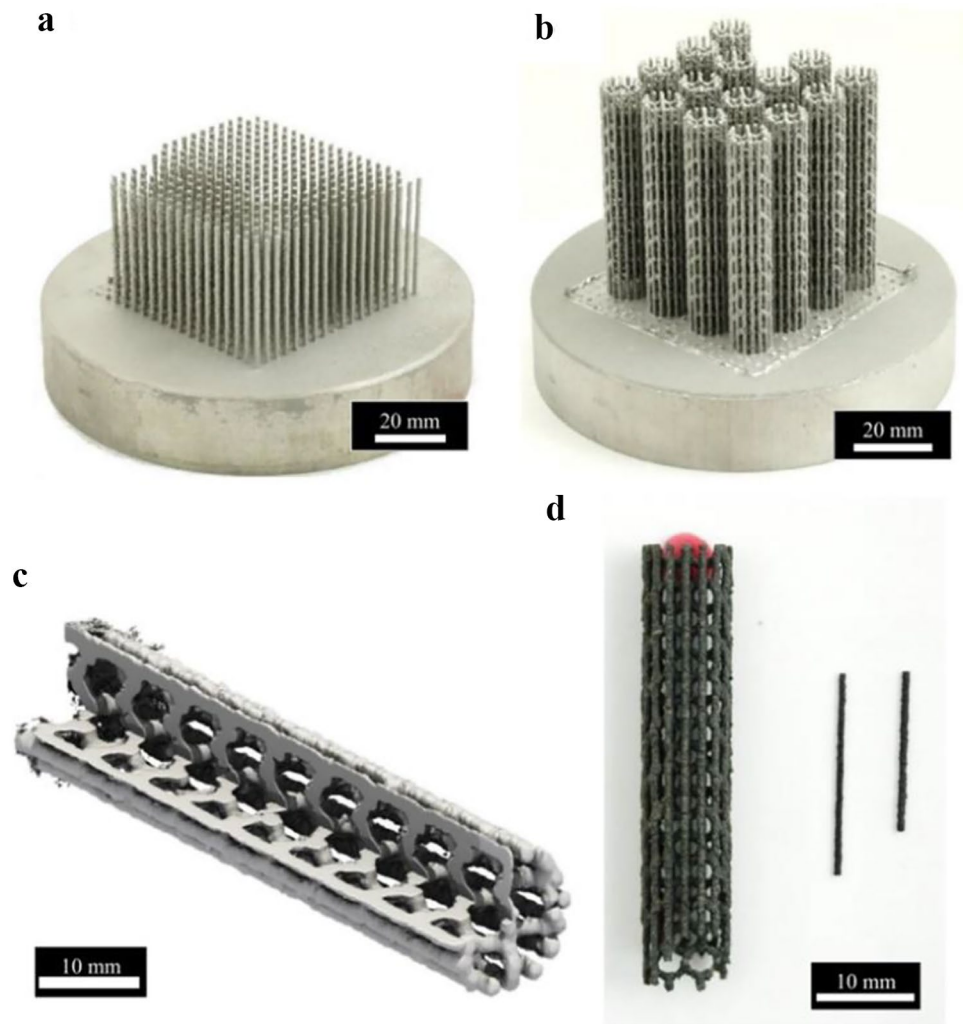
process window for EB-PBF is related to the sensitivity of the copper to thermal boundary conditions and geometric effects within a layer. Thus, while AM produces complex geometries from copper powder, the process parameter and properties data are typically associated with small prismatic specimens [39]. The AM process selection needs many cares and considerations to ensure the good quality and performance of the printed components. The reflectivity of the copper powder in an electron beam is quite lower than a laser; therefore, the efficiency of the EB-PBF is higher than that of laser-based systems. Higher preheat temperature in electron beam systems reduces the effect of periodic cooling and heating as well as the need for thermal processing to solve residual stress issues. This has culminated in the quality of EB-PBF parts in comparison with LB-PBF. Due to using a higher power energy source and larger beam size, the dimensional accuracy of EB-PBF is lower than LB-PBF.

Therefore, more post-processing to achieve surface quality and dimensional deviation is needed for the EB-PBF component that can add to the total manufacturing lead time and the cost of the production.

EB-PBF of unalloyed copper generally has fewer challenges compared to LB-PBF. The induced energy between the beam and the powder is significantly higher, the mid-level vacuum environment ($\sim 2 \times 10^{-3}$ to 2×10^{-6} mBar) minimises oxidation, and the high scan speed and beam power facilitate efficient bed preheating to reduce thermal gradients and residual stresses.

Pure copper has high thermal conductivity ($400\,\mathrm{W\,m^{-1}\,K^{-1}}$ at room temperature) which, while ideal for thermal management applications, promptly conducts heat away from the melt track leading to local thermal gradients. This phenomenon increases the chances of layer curling, delamination, and ultimately, component and builds failure. The resulting rapid

Table 2 Mechanical and physical properties of pure copper produced by EB-PBF

Method	Hatch (µm)	Thermal conductivity, W/(m.K)	Scanning speed (mm/s)	Micro hardness (VK)	Electrical conductivity (%IACS)	Power (W)	Layer thickness (µm)	Density%	Energy (j/mm^3)	Tensile strength (MPa)	Powder size (µm)	Year/ref
Electron beam powder bed fusion	100	403.55	250	-	94	275	50	99.5	220	-	-	[10]
	100	-	500	-	-	450	50	99.5	180	177 ±3.3	-	[10]
	100	408.27	1000	56.6±2.53	-	600	50	99.5	120	-	-	2018 [22]
	100	411.89	1500	55.5±1.64	100	850	50	-	113	-	-	[10]
	100	385.64	2000	57.8±1.55	100	1100	50	99.5	110	-	-	[10]
	100	400.1	3000	-	96.24	-	50	99.831	80	-	-	2016 [16]
	100	-	500	-	-	450	-	99.5	-	231.6±5.4	-	2020 [31]
	100	-	3000	-	-	-	50	99.5	0.275	-	10–50	2015 [40]
	100	-	80	88	-	-	-	-	-	-	60	2011 [49]
	-	390	-	-	97	-	-	99.32	-	76	-	2014[49]

solidification of the melt track, coupled with the low viscosity of melted copper, causes the lack of flowability of the material and also tends to retain defects such as keyholes [11]. Moreover, copper's high ductility prevents post-build powder removal and recovery which reduces the efficiency of the process. Copper powder particles also tend to agglomerate, reducing overall flowability and hindering powder deposition. Great care must be taken in storage and handling before, during and after part fabrication due to the sensitivity of copper to oxidation [35].

Key concerns when producing copper components by EB-PBF for fabrication of vacuum electronics parts are the requirements for high purity materials with small feature sizes, low surface roughness and ultra-high vacuum compatibility. The purity of the feedstock needs to be as high as possible. In addition, the material purity also needs to be preserved within the melting and solidification steps. In EB-PBF, even relatively low frequency (i.e. S-band) vacuum electron devices cause challenges in requiring small feature sizes and high surface quality (~ 1 µm) [48].

For particle accelerator applications, copper is commonly required to meet or exceed that of ASTM F68 for Class 1 oxygen-free electronic (OFE) copper, which is equivalent to 0.15176 ohms g/m^2 or 101.0% of the minimum International Annealed Copper Standard (IACS) at the ambient temperature [50]. The maximum allowable oxygen content for OFE copper should be 0.0005 wt% (5 wt. ppm). The negative influence of oxygen contamination on the thermal, electrical and mechanical properties of copper is small, but not negligible. The incoherent Cu_2O found along the grain boundaries has a similar effect as porosity and negatively affects the mechanical properties of the produced parts. For instance, electrolytic tough pitch copper has an oxygen content of ~ 0.04% (400 ppm) and typically exceeds 100–101% IACS. Another significant impact of oxygen content is the adverse effect of embrittlement in the copper parts during the downstream hydrogen brazing processes. The powder feedstock of EB-PBF is commonly subjected to oxygen contamination during transport, handling, loading, screening and loading after atomization. At ambient temperature, the oxygen solubility in pure copper is less than 2 wt. ppm, while the excess oxygen reacts to form a cuprous oxide, Cu_2O, as a non-passivating surface film or along the grain boundaries. At elevated temperatures (> 570 K), cupric oxide (CuO) and other variants may also form, which negatively affects the quality of the printed productions [11].

On the other hand, in EB-PBF, an electron beam is focused and accelerated to approximately half the speed of light and selectively melts successive layers of the powder. The absorptivity of the electron beam is higher than laser, and electromagnetic optics are used to focus and deflect the beam. This provides the possibility of much higher scan

speeds than laser-based systems, which facilitates periodic scanning of the entire build plate, thus maintaining an elevated temperature (~ 400–700 ℃ for copper), and virtually eliminating internal stresses caused by periodic heating [48].

5 Conclusion

This review aims to discuss the effect of printing conditions, process parameters, pre-processing and post-processing, as well as oxygen content (in powder and bulk material) on the microstructure, mechanical properties and quality of processes copper components by EB-PBF. The technical challenges of copper processing are identified to shed light on the process challenges and opportunities for EB-PBF processing. In this analysis, a roadmap is presented for the research contributions required to allow the commercial application of EB-PBF technologies.

- Copper and copper alloys have unique chemical and physical properties such as electrical and thermal conductivity, making them an ideal choice for many commercial applications such as electrical applications and building applications including fire sprinklers. However, the physical property of pure copper is greatly affected by impurities and contamination.

- Oxygen content in the EB-PBF of copper powder plays a significant role in the mechanical properties and quality of the printed parts. Powder with high oxygen content (0.0235%wt) has cracks, whereas specimens from the powder with low oxygen content are crack-free. The Cu_2O that appears in the process can improve the mechanical properties, while if the Cu_2O exceeds a certain percentage, cracks happen that negatively affect the mechanical properties. Hydrogen heat treatment reduces the amount of oxygen and related issues for the powder and subsequent components. The produced H_2O is also evaporated from the heat-affected zone and exits from the fume outlet.

- In copper printing by electron beam, the process parameters have to be maintained in such a way as to produce low build temperatures. This negates the high sintering tendency of the powder which is related to the high thermal conductivity of pure copper. An effective way to produce parts with homogeneity in mechanical properties is preheating. The temperature at the top of the meltpool is relatively higher than at the bottom of the substrate. Therefore, preheating in the range of 400–600 ℃ to produce a similar temperature for all areas of the meltpool is a practical solution.

- The highest electrical conductivities (58e6 S/m) were found for the samples with low porosity (less than 1%), while for samples with high porosity, electrical conductivities were found in the lowest value. Pores reduce the conductivity because of a reduction in conduction cross-section and electron transformation.

- The melting point of the material is an important governing factor for meltpool morphology and size. The role of the material thermal conductivity can outweigh the melting point and drive the meltpool size. The meltpool morphology and features drive the microstructure of copper parts in EB-PBF. Similar to LB-PBF, the microstructure of copper components by EB-PBF is highly driven by the size of the sample. In order to improve the mechanical properties and the quality of the printed components, post-processing has been suggested. HIP slightly improved sample density, while vacuum annealing reduced the oxygen content. As-built components are shown to have the highest yield strength, while post-processing including vacuum treatment and hot isostatic pressing improved the ductility and elongation. In a certain condition, the harder components can be obtained by EB-PBF. The hardness for precipitate-dislocation architectures was raised by 18.75% and 50% compared to full density copper EB-PBF and conventionally produced pure copper.

This paper shows that EB-PBF can successfully process copper for different parts and applications provided that proper care in the process is taken into account. EB-PBF showed a robust method to produce near-net or final shapes with comparable mechanical properties to conventional manufacturing such as casting and machining.

6 Future direction

Future work will be directed towards the numerical simulation of EB-PBF of copper components and detecting the underlying physics of this process for inter-layer and intra-layer regions. More study about the rheological properties of copper when changing process parameters, energy density and the temperature of the melt tracks will also provide unique and fundamental information on this process which can be another direction for the research on EB-PBF of copper. Investigating the effect of energy density and the dosimetry of the electron beam on the temperature of the copper material can shed light on this dynamic additive manufacturing process.

Appendix

Table A1 Outlines the chemical composition of various grades of copper alloys [23]

Family	CDA	AMS	UNS	Cu [%]	Sn [%]	Pb [%]	Zn [%]	Ni [%]	Fe [%]	Al [%]	Other [%]
Red brass	833		C83300	93	1.5	1.5	4				
			C83400 [7]	90			10				
	836	4855B	C83600	85	5	5	5				
	838		C83800	83	4	6	7				
Semi-red brass	844		C84400	81	3	7	9				
	845		C84500	78	3	7	12				
	848		C84800	76	3	6	15				
Manganese bronze			C86100 [8]	67	0.5		21		3	5	Mn 4
	862†		C86200	64			26		3	4	Mn 3
	863†	4862B	C86300	63			25		3	6	Mn 3
	865	4860A	C86500	58	0.5		39.5		1	1	Mn 0.25
Tin bronze	903		C90300	88	8		4				
	905	4845D	C90500	88	10	0.3 max	2				
	907		C90700	89	11	0.5 max	0.5 max				
Leaded tin bronze	922		C92200	88	6	1.5	4.5				
	923		C92300	87	8	1 max	4				
	926	4846A	C92600	87	10	1	2				
	927		C92700	88	10	2	0.7 max				
High-leaded tin bronze	932		C93200	83	7	7	3				
	934		C93400	84	8	8	0.7 max				
	935		C93500	85	5	9	1	0.5 max			
	937	4842A	C93700	80	10	10		0.7 max			
	938		C93800	78	7	15		0.75 max			
	943	4840A	C94300	70	5	25		0.7 max			
Aluminium bronze	952		C95200	88					3	9	
	953		C95200	89					1	10	
	954	4870B	C95400	85					4	11	
		4872B									
			C95410 [9]	85					4	11	Ni 2
	955		C95500	81				4	4	11	
			C95600 [11]	91						7	Si 2
			C95700 [12]	75				2	3	8	Mn 12
	958		C95800	81				5	4	9	Mn 1
Silicon bronze			C87200 [13]	89							Si 4
			C87400 [14]	83			14				Si 3
			C87500 [15]	82			14				Si 4
			C87600 [16]	90			5.5				Si 4.5
	878		C87800 [17]	80			14				Si 4
			C87900 [18]	65			34				Si 1

The chemical composition may vary to yield mechanical properties. Chemical composition of copper alloys

Availability of data and material Not applicable.

Code availability Not applicable.

Declarations

Ethics approval Not applicable.

Consent to participate Not applicable.

Consent for publication Not applicable.

Competing interests The authors declare no competing interests.

References

1. Oliveira J et al (2018) Laser welding of Cu-Al-Be shape memory alloys: microstructure and mechanical properties. Mater Des 148:145–152

2. Oliveira JP et al (2016) Improvement of damping properties in laser processed superelastic Cu-Al-Mn shape memory alloys. Mater Des 98:280–284

3. ASTM I (2015) ASTM52900–15 standard terminology for additive manufacturing—general principles—terminology. ASTM International, West Conshohocken, PA

4. Gibson I, Khorasani AM (2019) Metallic additive manufacturing: design, process, and post-processing. Multidisciplinary Digital Publishing Institute

5. Pérez-Ruiz JD et al (2021) On the relationship between cutting forces and anisotropy features in the milling of LPBF Inconel 718 for near net shape parts. Int J Mach Tools Manuf 170:103801

6. Pérez-Ruiz JD et al (2022) Stiffening near-net-shape functional parts of Inconel 718 LPBF considering material anisotropy and subsequent machining issues. Mech Syst Signal Process 168:108675

7. González-Barrio H et al (2022) Hybrid manufacturing of complex components: full methodology including laser metal deposition (LMD) module development, cladding geometry estimation and case study validation. Mech Syst Signal Process 179:109337

8. Gorji N, O'connor R, Brabazon D (2021) XPS, SEM, AFM, and nano-indentation characterization for powder recycling within additive manufacturing process. in IOP Conference Series: Materials Science and Engineering. IOP Publishing

9. Gibson I et al (2021) Powder bed fusion. Additive Manufacturing Technologies. Springer, pp 125–170

10. Jiang Q et al (2021) A review on additive manufacturing of pure copper. Coatings 11(6):740

11. Ledford C et al (2019) Characteristics and processing of hydrogen-treated copper powders for EB-PBF additive manufacturing. Appl Sci 9(19):3993

12. Huang J et al (2020) Pure copper components fabricated by cold spray (CS) and selective laser melting (SLM) technology. Surf Coat Technol 395:125936

13. Constantin L et al (2020) Laser 3D printing of complex copper structures. Addit Manuf 35:101268

14. Walker DC, Caley WF, Brochu M (2014) Selective laser sintering of composite copper–tin powders. J Mater Res 29(17):1997–2005

15. Zhong H et al (2018) The graded microstructures evolving with thermal cycles in pure copper processed by laser metal deposition. Mater Lett 230:215–218

16. Raab SJ et al (2016) Thermal and electrical conductivity of 99.9% pure copper processed via selective electron beam melting. Adv Eng Mater 18(9):1661–1666

17. Körner C (2016) Additive manufacturing of metallic components by selective electron beam melting—a review. Int Mater Rev 61(5):361–377

18. Bardakhanov S et al (2015) Channel structures formed in copper ingots upon melting and evaporation by a high-power electron beam. Metals 5(1):428–438

19. Gibson I et al (2021) Additive manufacturing technologies. Vol. 17. Springer

20. Jadhav SD et al (2019) Influence of carbon nanoparticle addition (and impurities) on selective laser melting of pure copper. Materials 12(15):2469

21. Ikeshoji T-T et al (2018) Selective laser melting of pure copper. Jom 70(3):396–400

22. Guschlbauer R et al (2018) Process development of 99.95% pure copper processed via selective electron beam melting and its mechanical and physical properties. Mater Charact 143:163–170

23. Brass and bronze alloys (2009) archived from the original on 2009–08-25, retrieved. Schumann, Germany

24. Colopi M et al (2019) Limits and solutions in processing pure Cu via selective laser melting using a high-power single-mode fiber laser. The International Journal of Advanced Manufacturing Technology 104(5):2473–2486

25. Yan X et al (2020) Microstructure and mechanical properties of pure copper manufactured by selective laser melting. Mater Sci Eng, A 789:139615

26. Pobel CR, Lodes MA, Körner C (2018) Selective electron beam melting of oxide dispersion strengthened copper. Adv Eng Mater 20(8)

27. Vutova K et al (2012) Influence of process and thermo-physical parameters on the heat transfer at electron beam melting of Cu and Ta. in 141st Annual Meeting and Exhibition, TMS 2012. Orlando, FL: Minerals, Metals and Materials Society

28. Ramirez DA et al (2011) Open-cellular copper structures fabricated by additive manufacturing using electron beam melting. Mater Sci Eng, A 528(16–17):5379–5386

29. Momeni S et al (2018) Selective electron beam melting of a copper-chrome powder mixture. Mater Lett 223:250–252

30. Guschlbauer R et al (2020) Effect of the oxygen content of pure copper powder on selective electron beam melting. Mater Sci Eng A 779

31. Lodes MA, Guschlbauer R, Körner C (2015) Process development for the manufacturing of 99.94% pure copper via selective electron beam melting. Mater Lett 143:298–301

32. Lippold JC (2014) Welding metallurgy and weldability. John Wiley & Sons

33. Laporte V, Mortensen A (2009) Intermediate temperature embrittlement of copper alloys. Int Mater Rev 54(2):94–116

34. Juechter V et al (2014) Processing window and evaporation phenomena for Ti–6Al–4V produced by selective electron beam melting. Acta Mater 76:252–258

35. Frigola P et al (2014) Fabricating copper components with electron beam melting. Adv Mater Processes 172(7):20–24

36. Cheng B, Chou K (2018) A numerical investigation of thermal property effects on melt pool characteristics in powder-bed electron beam additive manufacturing. Proceedings of the Institution of Mechanical Engineers, Part B: Journal of Engineering Manufacture 232(9):1615–1627

37. Cheng B et al (2014) On process temperature in powder-bed electron beam additive manufacturing: model development and validation. J Manuf Sci Eng 136(6)

38. Dye D et al (2001) Modeling of the mechanical effects induced by the tungsten inert-gas welding of the IN718 superalloy. Metall and Mater Trans A 32(7):1713–1725

39. Tarafder P, Rock C, Horn T (2021) Quasi-static tensile properties of unalloyed copper produced by electron beam powder bed fusion additive manufacturing. Materials 14(11)

40. Ramirez D et al (2011) Novel precipitate–microstructural architecture developed in the fabrication of solid copper components by additive manufacturing using electron beam melting. Acta Mater 59(10):4088–4099

41. Ledford C et al (2020) Evaluation of electron beam powder bed fusion additive manufacturing of high purity copper for overhang structures using in-situ real time backscatter electron monitoring. Procedia Manufacturing 48:828–838

42. Lomakin K et al (2019) 3D Printed copper waveguides by selective electron beam melting process for e-band. in 49th European Microwave Conference, EuMC 2019. Institute of Electrical and Electronics Engineers Inc

43. Sanchez J, Murr L, Staudhammer K (1997) Effect of grain size and pressure on twinning and microbanding in oblique shock loading of copper rods. Acta Mater 45(8):3223–3235

44. Wen S et al (2013) Thermal contact resistance between the surfaces of silicon and copper crucible during electron beam melting. Int J Therm Sci 74:37–43

45. Calleja-Ochoa A et al (2021) A new approach in the design of microstructured ultralight components to achieve maximum functional performance. Materials 14(7):1588

46. Wolf T et al (2020) Periodic open cellular Raney-Copper catalysts fabricated via selective electron beam melting. Adv Eng Mater 22(5)

47. Yu Y et al (2020) Modeling precipitation process of Al-Cu alloy in electron beam selective melting with a 3D cellular automaton model. Additive Manufacturing 36

48. Gamzina D et al (2018) Additive vacuum electronics: electron beam melting of copper. in 18th International Vacuum Electronics Conference, IVEC 2017. Institute of Electrical and Electronics Engineers Inc

49. Frigola P et al (2014) Fabricating copper components. Adv Mater Process 20

50. Davis JR (2001) Copper and copper alloys. ASM international

Publisher's Note Springer Nature remains neutral with regard to jurisdictional claims in published maps and institutional affiliations.